PROCEEDINGS, Thirty-Second Workshop on Geothermal Reservoir Engineering
Stanford University, Stanford, California, January 22-24, 2007
SGP-TR-183

NUMERICAL SIMULATION OF TRACER TESTING DATA AT THE UENOTAI GEOTHERMAL FIELD, JAPAN

Shinsuke Nakao, Tsuneo Ishido and Yoshinobu Takahashi*

Geological Survey of Japan, AIST
AIST Central 7
Tsukuba, Ibaraki, 305-8567, Japan
e-mail: sh-nakao@aist.go.jp

* Akita Geothermal Energy Corporation
21 Shimono, Takamatsu
Yuzawa, Akita, 019-0404, Japan

ABSTRACT

Numerical simulation of tracer testing data is conducted based on hydrogeology parameters inferred from pressure interference data. By incorporating both of pressure interferences and tracer testing data, pertinent values of average fracture spacing and rock-matrix permeability can be estimated. Relatively good match of tracer return curves are obtained. It is necessary to assign very small fracture porosity (product of fracture-zone porosity and fracture-zone volume fraction) between wells in order to match tracer return curves. Our 3-D simulation model predicts a large-scale distribution of two-phase zone due to production; this is partly confirmed by a good match between the observed and calculated discharge enthalpy of the production well.

INTRODUCTION

The Uenotai geothermal field is located in northern Honshu, Japan, where a 27.5 MW geothermal power station has been operated by Akita Geothermal Energy Corporation since 1994. The Uenotai geothermal system is a liquid-dominated system with a central zone of aquifer boiling. The two-phase reservoir has evolved from liquid in the natural state due to exploitation (Takeno, 2000). In northwestern area of the field (Figure 1), downhole pressure interference data of well D-2 has been obtained during reinjection into well D-1 and productions from T-41, E-2, etc. since 2001. Tracer test was also conducted using two-phase tracers (methanol and ethanol) and liquid phase tracer (xylenesulfonate) in 2002 to check the connectivity among the reinjection well and production wells in the vicinity of the NW area. Such kind of information is useful to refine the reservoir model.

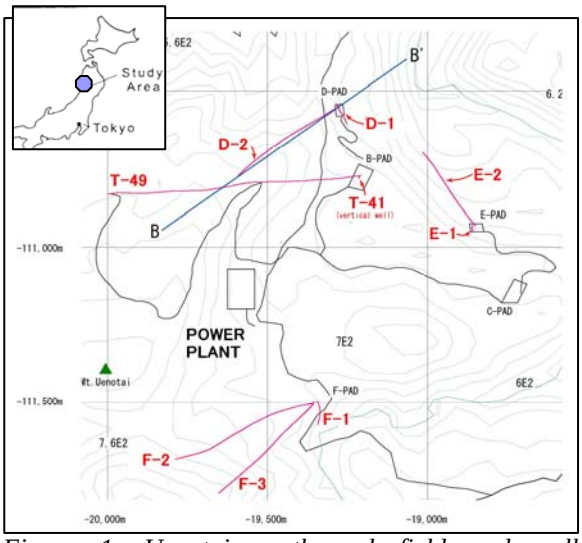

Figure 1. Uenotai geothermal field and well locations.

Stability of alcohols as two-phase tracers was reported by Adams (1995) and Adams et al. (2000). Because methanol is the most stable of the alcohols with no decay being detected from a two-week run at 320 ^{o}C and a pH of 4 (Adams et al, 2000), we will focus on the numerical simulation of tracer tests using methanol. Mathematical representation of phase-partitioning tracers in numerical simulations was presented by Trew et al. (2001) and Pruess et al. (2002). Field observation of tracer tests and numerical simulation using alcohols in Japan were reported by Fukuda et al. (2005) and Sato et al. (2005), respectively.

In this paper, we will briefly describe analyses of pressure interference data. Then we will present a result of reproducing discharge enthalpy of a production well and tracer test data by using a three-dimensional numerical simulation model.

PRESSURE INTERFERENCE DATA

Downhole pressure interference data of well D-2 has been obtained during reinjections into well D-1 since 2001. Figure 2 shows an example of flow-rate histories of water injection into well D-1 and corresponding pressure interference observed in well D-2. Total depths of well D-1 and D-2 are 855 m and 1705 m, respectively. A pressure gauge was installed at the depth of 1010 m in D-2. The horizontal distance of main feed zones between well D-1 and D-2 is approximately 200 m.

Different pulse flow-rate periods (both of shut-in and injection periods) of well D-1 were selected and corresponding time lags in pressure interference of well D-2 were measured. The hydraulic diffusivity value for each pulse period was calculated based on the approach by Nakao et al. (2005). These hydraulic diffusivity values versus pulse flow-rate periods are plotted in Figure 3. It can be seen that the hydraulic diffusivity calculated from the observed data decreases as the pulse flow-rate period increases, suggesting the medium between the two wells is fractured type. A fitting curve (dashed line in Figure 3) reaches a steady value (0.8 m^2/s) when pulse flow-rate period becomes more than 340 hours; this time corresponds to τ_p (the time required for pressure equilibrium between the fracture zones and rock matrix). For spherical rock matrix blocks,

$$\tau_p = \frac{\phi_m C_t \mu x_m^2}{10\, k_m} \qquad (1)$$

where x_m is average fracture spacing; C_t is a total compressibility; ϕ_m and k_m represent the porosity and permeability of rock matrix, respectively.

If we assume that the porosity and permeability of the rock matrix are 0.05 and 10^{-19} - 10^{-17} m^2 respectively, the average fracture spacing (x_m) is estimated to be 14 - 135 meters from Equation 1, where μ = 1.05 x 10^{-4} (Pa-s) and C_t = 1.7 x 10^{-9} (Pa^{-1}) at the temperature of 260 ^oC are used.

An inversion analysis of the whole pressure interference data is also conducted by using the inversion program DIAGNS (Garg et al., 2002), which employs an iterative least-squares approach. The pressure response of well D-2 to injection into well D-1 as shown in Figure 2 was fit using both a line-source single-porosity (porous) model and a Warren-Root double-porosity model (Warren and Root, 1963).

The fracture spacing (x_m) can be also calculated from the value of fracture parameters λ (transmissivity ratio), which is derived form the inversion analysis of the whole pressure interference data. If the rock matrix blocks are cubes or spheres, λ is given by:

$$\lambda = \frac{60}{x_m^2} \frac{k_m}{k} r_w^2 \qquad (2)$$

where r_w is wellbore radius and k is total radial permeability (e.g. Kazemi, 1969). As a result of inversion analysis the λ and kh are estimated as 5.5 x 10^{-7} and 1.1 x 10^{-13} m^3 respectively. If we assume the formation thickness and the rock matrix permeability are 250 m and 10^{-19} - 10^{-17} m^2 respectively, the fracture spacing is evaluated as 16 - 155 m (r_w = 0.1 m). These values are consistent with those detected from the pulse testing analysis. The formation thickness of 250 m covers the vertical distance between main feedpoints of wells D-1 and D-2.

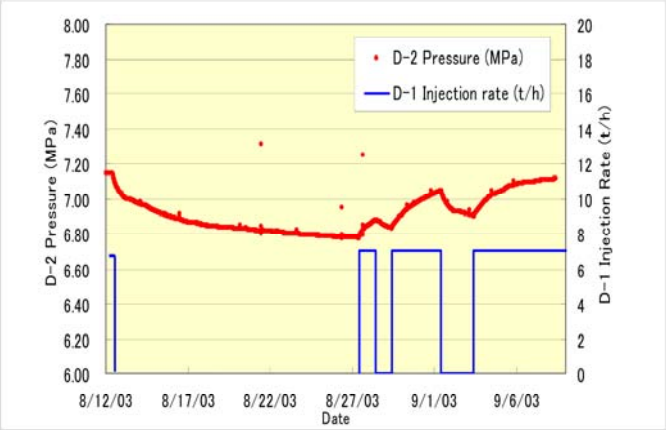

Figure 2. Histories of well D-2 downhole pressure, and injection flow-rates of well D-1.

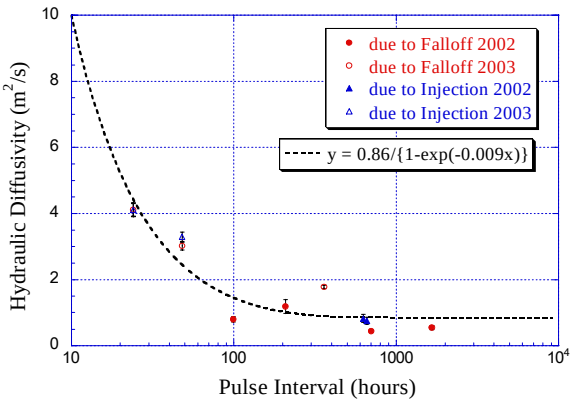

Figure 3. Dependence of hydraulic diffusivity on pulse flow-rate periods of the Uenotai geothermal field.

TRACER TEST DATA

Tracer testing was conducted in 2002 in the NW area of the Uenotai field. Two-phase tracers (methanol: 810 kg and ethanol: 810 kg) and a liquid-phase tracer (xylenesulfonate: 400 kg) were injected into well D-1. Both of the two-phase and liquid-phase tracers returned to the production well T-41 after nearly 70 hours. On the other hand, only two-phase tracers returned to the production well E-2 after approximately 85 hours, suggesting high vapor-phase saturation around well E-2. The tracer test results are summarized in Table 1.

Table 1. Result of tracer tests at the Uenotai field.

Production Well	Return Status		Initial Detection Time (h)	Recovery (%)
E-2	Methanol	O	85	43
Water : 0t/h	Ethanol	O		14
Steam : 24t/h	Xylene-sulfonate	X		-
T-41	Methanol	O	70	20
Water : 2.4t/h	Ethanol	O		11
Steam : 7.7t/h	Xylene-sulfonate	O		15

MODEL DESCRIPTION

For our numerical simulation study, we used the STAR general-purpose geothermal reservoir simulator (Pritchett, 1995). We used a 3-D reservoir geometry, as illustrated in Figure 4. The reservoir model consists of two parts; low-permeability upper three layers and relatively high-permeability lower seven layers (reservoir), dipping 15 degrees to the Y (N-W) direction. Solid circles and open circles in Figure 4 indicate injection points of the injection wells and feed points of the production wells, respectively. The kh, storativity and rock properties estimated from well tests are taken into account in constructing the model. The reservoir is treated as a "MINC"-type (Pruess and Narasimhan, 1985) fracture/matrix composite representation with fracture spacing (x_m) of 15 meters and rock matrix permeability (k_m) of 10^{-19} m^2 (Case 1), which is a possible combination of x_m and k_m as discussed in the previous section. We also carried out a sensitivity analysis using a model with fracture spacing of 40 meters and rock matrix permeability of 10^{-18} m^2 (Case 2).

Initial and boundary conditions are as follows. Impermeable conductive boundaries with the temperature of 270 ^oC and 300 ^oC are assigned at the

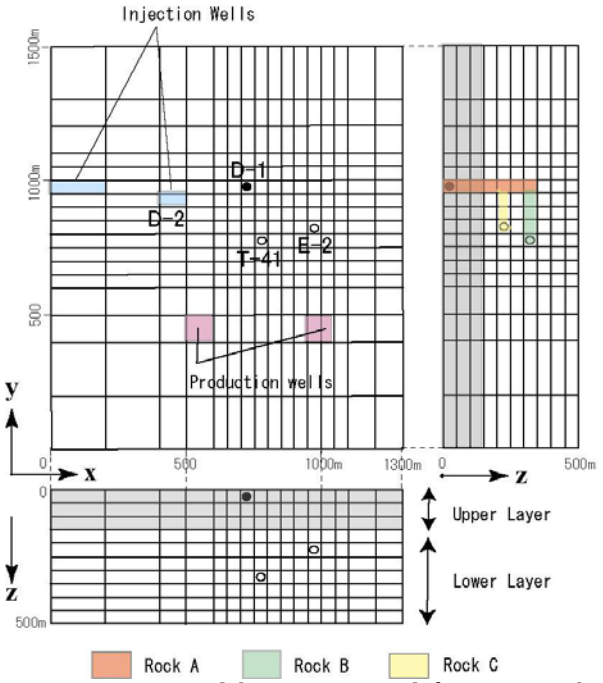

Figure 4. 3-D model geometry used for numerical simulation of tracer testing.

top and bottom boundaries, respectively. Constant temperature and pressure (260 ^oC, 7.5 - 10.9 MPa according to the depth) are specified for the side face of the reservoir at Y = 1500 m. Other boundaries are impermeable and insulated. A 300 ^oC mass source (10 kg/s) is assigned in ten grid blocks of the bottom layer at Y = 0. Uniform temperature of 260 ^oC and corresponding hydrostatic pressure distribution are applied to the entire model at the beginning. From the initial conditions described above, the fluid and heat flow were calculated for more than 1 x 10^4 years to reach a quasi-steady state, which was assumed as a starting model for exploitation calculations (Fig. 6a).

Linear relative permeability curves are assumed with residual vapor saturation (S_{rv}) and residual liquid saturation (S_{rl}) being 0.05 and 0.3, respectively. Whether such assumption is applicable here is not pertinent to the present study, although the subject itself is very important.

In the STAR code, user-specified partition functions (mass fraction of tracer in vapor phase/mass fraction of tracer in liquid phase) are regarded as functions of temperature. Because a steam to liquid concentration ratio of five to fifteen may be reached for ethanol at geothermal injection temperatures (Adams et al., 2000), we simply set a partition function of methanol to be 10 in the present study. We ignore processes which can destroy tracers through chemical reactions, or which involve tracer mass interchange between the fluid phases and the surrounding rock. That is, the conservative tracers are assumed.

Table 2. Rock properties of the 3-D model.

Reservoir Geometry	Dimensions (m)	1300 x 1500 x 500
	Grid Blocks	16 x 17 x 10

Rock Properties

	Upper Layer	Lower Layer	Rock A	Rock B	Rock C
Permeability (m^2):	1.0×10^{-15}	5.0×10^{-15}	1.0×10^{-14}	3.0×10^{-14}	5.0×10^{-15}
Fracture Volume Fraction	0.05	0.05	0.02	0.02	0.1
Fracture Porosity	0.05	0.05	0.05	0.05	0.05
Rock Matrix Permeability (m^2): Case1	1.0×10^{-19}	1.0×10^{-19}	1.0×10^{-19}	1.0×10^{-19}	1.0×10^{-19}
Case2	1.0×10^{-18}	1.0×10^{-18}	1.0×10^{-18}	1.0×10^{-18}	1.0×10^{-18}
Fracture Spacing (m): Case 1	15	15	15	15	15
Case 2	40	40	40	40	40
Rock Matrix Porosity	0.05	0.05	0.05	0.05	0.05

Numerical simulations are performed in two stages. Firstly we try to match histories of production wells, such as flow-rates and discharge enthalpy, using two-layer rock properties. Secondly we aim to match two-phase tracer test results by adjusting interwell permeability and fracture porosity with Rocks A, B and C (Table 2).

RESULT AND DISCUSSION

To simulate power plant operation, we used "power systems" module in the STAR code. Totally ten years are simulated starting from November, 1993. Production well T-41 is activated two years later from time zero to provide "desired output power" of 3 MWe. Production well E-2 is added to provide 5 MWe after 7 years. Tracers are injected into well D-1 after 8.5 years. Figure 5 illustrates simplified field observation of flow-rate histories of three wells located in the main NW area. Production flow-rates of wells E-2 and T-41 are free parameters to be matched in the simulation by adjusting a productivity index etc. To reproduce excess enthalpy of the production well E-2, histories of production wells within the central area, of which locations are shown as red-colored grid blocks in Figure 4, are also incorporated in the model.

After matching discharge enthalpy and flow-rate of the production wells, matching of tracer return curves is conducted by adjusting permeabilities and fracture porosities between the production and injection wells. In order to match tracer testing data, it is necessary to assign very small fracture porosity (product of fracture-zone porosity and fracture-zone volume fraction) between wells, which is less than 0.01.

Figure 6(b) shows distributions of pressure (black), temperature (red) and vapor-phase saturation (yellow) in a NW-SE vertical section passing well E-2 after 8.5 years of operation. The yellow-colored area represents that the vapor-phase saturation is larger than 0.2. Figure 6(a) shows distributions of the starting model for the purpose of reference. Two pressure and temperature anomalies shown in Figure 6(b) correspond to the NW and central production zones. Calculated total vapor-phase volume in all grid blocks increases with time (Figure 7). With the increase of vapor-phase volume due to production, excess enthalpy of the production well E-2 can be reproduced.

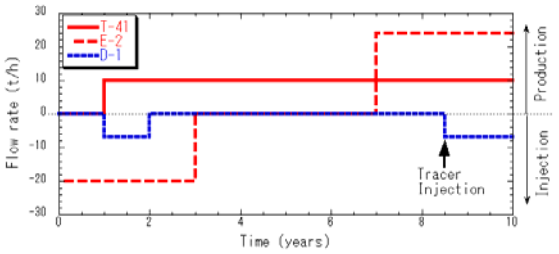

Figure 5. Simplified flow-rate histories of three wells in the main NW area. Note that the flow-rates of the production wells are parameters in the numerical simulation.

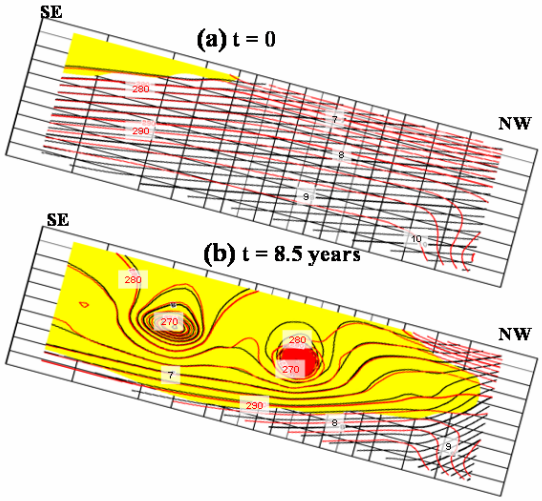

Figure 6. Distributions of pressure (black), temperature (red) and vapor-phase saturation larger than 0.2 (yellow) in a NW-SE vertical section passing well E-2: (a) at t =0, (b) after t = 8.5 years.

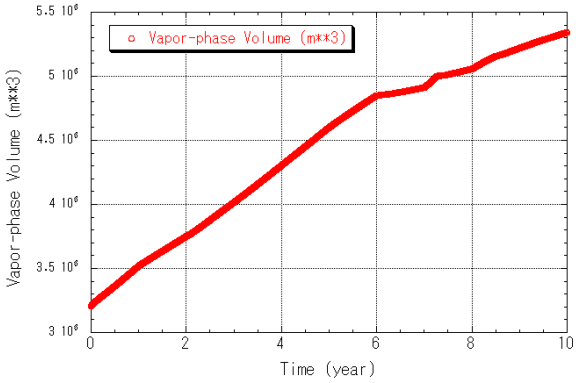

Figure 7. Calculated change of total vapor-phase volume in all grid blocks.

Figure 8 and Figure 9 illustrate comparisons of flow rate, discharge enthalpy, and return curve of two-phase tracer (methanol) between observed data and calculations for well E-2. A better match is achieved for Case 1 (with x_m = 15 m and $k_m = 10^{-19}$ m^2) than Case 2 (with x_m = 40 m and $k_m = 10^{-18}$ m^2). Three fractured rocks A, B and C between the wells are adopted to express unknown preferential flow paths. The calculated tracer return curve cannot be matched to the observed data without adopting the three fractured rocks as shown in Figure 9, although it does not affect the discharge enthalpy. A calculated peak value of liquid-phase tracer return is 1.5 ppm, which is consistent with the fact that only two-phase tracers return were observed at well E-2.

As for well T-41, the calculated discharge enthalpy becomes much lower than the observed data. The structure around well T-41 is thought to be too simple to reproduce well T-41 behaviors.

CONCLUDING REMARKS

The 3-D numerical simulation of tracer tests is conducted in order to construct advanced reservoir models and investigate the distribution of vapor-phase saturation. Relatively good match of tracer return curves is obtained between well D-1 and well E-2. In order to match tracer return curves, it is necessary to assign very small fracture porosity (product of fracture-zone porosity and fracture-zone volume fraction) between wells, which is less than 0.01.

Our simulation model has a large-scale distribution of two-phase zone due to productions both in the NW area and the central area, resulting in reproducing high discharge enthalpy of the production well E-2. By incorporating both of pressure interferences and tracer testing data, average fracture spacing (x_m = 15 m) and rock-matrix permeability ($k_m = 10^{-19}$ m^2) are estimated.

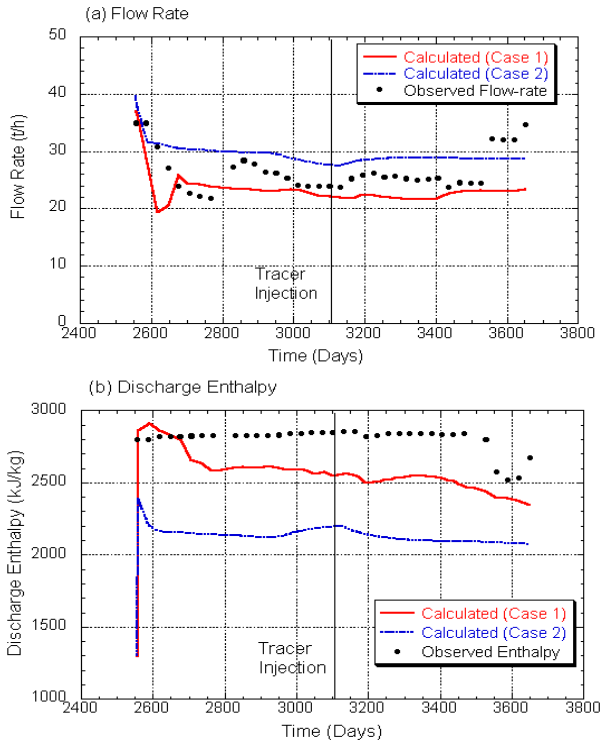

Figure 8. Observed and calculated (a) flow rate and (b) discharge enthalpy of well E-2: Case 1 (x_m = 15 m, $k_m = 10^{-19}$ m^2), Case 2 (x_m = 40 m, $k_m = 10^{-18}$ m^2).

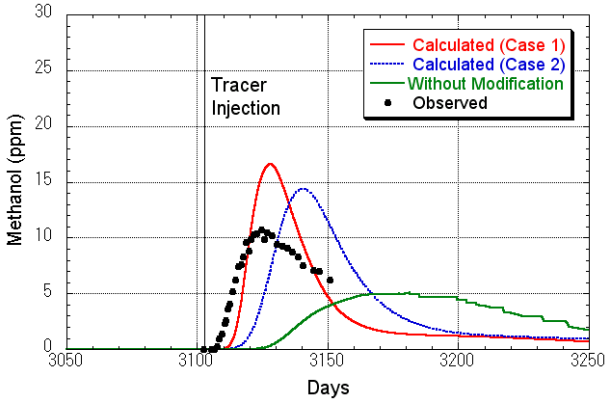

Figure 9. Observed and calculated two-phase tracer return curve of well E-2: Case 1 (x_m = 15 m, $k_m = 10^{-19}$ m^2), Case 2 (x_m = 40 m, $k_m = 10^{-18}$ m^2) and the case without modification of rocks A, B and C.

ACKNOWLEDGEMENTS

This work was conducted as part of collaborative research works between Akita Geothermal Energy Co., Ltd. and Geological Survey of Japan, AIST. The authors would like to thank Akita Geothermal Energy Co., Ltd. for permission to use data from the Uenotai geothermal field.

REFERENCES

Adams, M. C. (1995), "Vapor, Liquid, and Two-phase Tracers for Geothermal Systems," *Proc. World Geothermal Congress 1995*, 1875-1880.

Adams, M. C., Yamada, Y., Yagi, M., Kondo, T. and Wada, T. (2000), "Stability of Methanol, Propanol, and SF_6 as High-temperature Tracers," *Proc. World Geothermal Congress 2000*, 3015-3019.

Fukuda, D., Asanuma, M., Hishi, Y. and Kotanaka, K. (2005), "The First Two-phase Tracer Tests at the Matsukawa Vapor-dominated Geothermal Field, Northeast Japan," *Proc. World Geothermal Congress 2005*, Paper No. 1204.

Garg, S. K., Alexander, J. H., Ellis, M., Kelly, C., Kuharski, R. and Patnaik, P. (2002), "*Well Testing for Hydrological Properties: Geothermal Pressure Transient Analysis Software DIAGNS (FY2001)*", SAIC-02/1011.

Kazemi, H. (1969), "Pressure Transient Analysis of Naturally Fractured Reservoirs with Uniform Fracture Distribution", *Soc. Pet. Eng. J.*, **9**, 451-462.

Nakao, S., Ishido, T., Hatakeyama, K. and Ariki, K. (2005), "Analysis of Pulse Tests in a Fractured Geothermal Reservoir – A Case Study at the Sumikawa Field in Japan," *Proc. World Geothermal Congress 2005*, Paper No. 1137.

Pritchett, J. W. (1995), "*STAR User's Manual*", Report SSS-TR-92-13366, S-Cubed, La Jolla, Calif, 312p.

Pruess, K. (2002), "Numerical Simulation of 'Multiphase Tracer Transport in Fractured Geothermal Reservoirs," *Geothermic*, **31**, 475-499.

Pruess, K. and Narasimhan, T. N. (1985), "A Practical Method for Modeling Fluid and Heat Flow in Fractured Porous Media", *Soc. Pet. Eng. J.*, Feb., 14-26.

Sato, K., Sakagawa, and Omiya, T. (2005), "Numerical Simulation of Liquid and Two-phase Tracers in a Part of the Kakkonda Geothermal Field, Japan," *Proc. 30th Workshop on Geothermal Reservoir Engineering*, Stanford University, 237-243.

Takeno, N. (2000), "Thermal and Geochemical Structure of the Uenotai Geothermal System, Japan", *Geothermics*, **29**, 275-277.

Trew, M., O'Sullivan, M. Harvey, M., Anderson, E. and Pruess, K. (2001), "Modeling the Phase Partitioning Behavior of Gas Tracers under Geothermal Reservoir Conditions," *Geothermics*, **30**, 655-695.

Warren J. E. and Root, P. J. (1963), "The Behavior of Naturally Fractured Reservoirs", *Soc. Pet. Eng. J.*, **3**, 245-255.